Extracellular vesicles promote lipid raft formation in human microglia through TLR4, P2X4R, and αVβ3/ αVβ5 signaling pathways

Augustas Pivoriūnas (augustas.pivoriunas@imcentras.lt)
State Research Institute Center for Innovative Medicine

Research Article

Keywords: Extracellular vesicles, lipid rafts, microglia, TLR4, P2X4R, cilengitide

Posted Date: October 28th, 2022

DOI: https://doi.org/10.21203/rs.3.rs-2212037/v1

Extracellular vesicles promote lipid raft formation in human microglia through TLR4, P2X4R, and αVβ3/αVβ5 signaling pathways.

Diana Romenskaja[1], Ugnė Jonavičė[1], Virginijus Tunaitis[1], Augustas Pivoriūnas[1*]

**-presenting author;*
1-Department of Stem Cell Biology, State Research Institute Centre for Innovative Medicine, LT-01102, Vilnius, Lithuania;

Abstract

Targeting of disease-associated microglia represents a promising therapeutic approach that can be used for the prevention or slowing down neurodegeneration. In this regard, the use of extracellular vesicles (EVs) represents a promising therapeutic approach. However, the molecular mechanisms by which EVs regulate microglial responses remain poorly understood. In the present study, we used EVs derived from human oral mucosa stem cells (OMSCs) to investigate the effects on the lipid raft formation and the phagocytic response of human microglial cells. Lipid raft labeling with fluorescent cholera toxin subunit B conjugates revealed that both EVs and lipopolysaccharide (LPS) by more than 2 times increased lipid raft formation in human microglia. By contrast, combined treatment with LPS and EVs significantly decreased lipid raft formation indicating possible interference of EVs with the process of LPS-induced lipid raft formation. Specific inhibition of Toll-like receptor 4 (TLR4) with anti-TLR4 antibody as well as inhibition of purinergic P2X4 receptor (P2X4R) with selective antagonist 5-BDBD inhibited EVs- and LPS-induced lipid raft formation. Selective blockage of αvβ3/ αvβ5 integrins with cilengitide suppressed EV- and LPS-induced lipid raft formation in microglia. Furthermore, inhibition of TLR4 and P2X4R prevented EV-induced phagocytic activity of human microglial cells.
We demonstrate that EVs induce lipid raft formation in human microglia through interaction with TLR4, P2X4R, and αVβ3/αVβ5 signaling pathways. Our results provide new insights about the molecular mechanisms regulating EV/microglia interactions and could be used for the development of new therapeutic strategies against neurological disorders.

Keywords: Extracellular vesicles; lipid rafts; microglia; TLR4; P2X4R; cilengitide.

Introduction

Microglial cells are key regulators of immune homeostasis in the central nervous system (CNS) (Augusto-Oliveira, Arrifano et al. 2022). Dysregulation of microglial function has been associated with pathogenesis of many neurological disorders, therefore targeting disease-associated microglia represents a promising therapeutic approach that can be used for the prevention or slowing down neurodegeneration and disease progression (Ransohoff 2016, Song and Colonna 2018).

Over the last few years, extracellular vesicles (EVs) attracted a significant interest as a potential therapy against various neurological conditions (Jarmalaviciute and Pivoriunas 2016, Wiklander, Brennan et al. 2019). EVs have several important advantages over traditional therapies because they can cross the blood-brain barrier (BBB) (Alvarez-Erviti, Seow et al. 2011) and also can be delivered into the brain by the minimally invasive intranasal routes (Narbute, Pilipenko et al. 2019, Herman, Fishel et al. 2021, Li, Wu et al. 2022). Furthermore, EVs can specifically target and accumulate in pathologically affected areas of the brain by yet unknown mechanisms (Guo, Perets et al. 2019, Perets, Betzer et al. 2019). Several reports demonstrated that EVs can be selectively internalized by the microglial cells and suppress activation and secretion of pro-inflammatory cytokines (Long, Upadhya et al. 2017, Losurdo, Pedrazzoli et al. 2020). However, the molecular mechanisms by which EVs regulate microglial responses still remain poorly understood.

Recent findings demonstrated a critical role of lipid rafts as a key components during the inflammatory response of glial cells (Miller, Navia-Pelaez et al. 2020, Sviridov, Mukhamedova et al. 2020). Lipid rafts are plasma membrane microdomains enriched in the sphingolipids, cholesterol, and associated proteins (Sezgin, Levental et al. 2017). Different inflammatory stimuli induce rapid enlargement of lipid rafts that serve as organizing platforms bringing together important regulators of inflammation and initiating an inflammatory response. These so-called inflammarafts are enriched in the innate immune receptors TLRs 2 and 4, TREM2, IFNγR, purinergic receptors P2X and P2Y, and integrins (Miller, Navia-Pelaez et al. 2020, Sviridov, Mukhamedova et al. 2020). It has been demonstrated that TLR4 expressed by the spinal microglia is crucial for the neuroinflammatory sensitization of central pain signaling pathways (Miller, Navia-Pelaez et al. 2020). Lipid rafts create a membrane microenvironment that supports TLR4 receptor dimerization, a critical step in TLR4 activation (Plociennikowska, Hromada-Judycka et al. 2015). Apolipoprotein A-I binding protein (AIBP) removed the excess cholesterol from the plasma membrane thereby reducing lipid raft formation and TLR4

dimerization (Woller, Choi et al. 2018). Intrathecal AIBP injections suppressed TLR4 dimerization, neuroinflammation and alleviated neuropathic pain in mice (Woller, Choi et al. 2018).

Microglial purinergic P2X4 receptors are important regulators for pain hypersensitivity, phagocytosis, and migration (Ohsawa, Irino et al. 2007, Ulmann, Hatcher et al. 2008, Zabala, Vazquez-Villoldo et al. 2018). Several studies demonstrated that the association of P2X4 and P2X7 receptor complexes with lipid rafts was required for the initiation of downstream signaling pathways (Garcia-Marcos, Dehaye et al. 2009, Suurvali, Boudinot et al. 2017, Kopp, Krautloher et al. 2019). Stimulation of microglia with LPS increased the fraction of the P2X4 receptors at the plasma membrane (Boumechache, Masin et al. 2009).

Integrin compartmentalization in lipid rafts is also necessary for proper cell adhesion and signaling (Lietha and Izard 2020). Lipid raft-mediated partitioning of activated integrins is important for the specific interaction with other signaling proteins (Green, Zheleznyak et al. 1999).

Our previous findings demonstrate that EVs may act as potent immunomodulators of human microglia by suppressing TLR4/ NFκB signaling pathway, promoting phagocytosis, and inducing metabolic reprogramming (Jonavice, Tunaitis et al. 2019). More recently we demonstrated that EVs derived from the dental pulp of human exfoliated deciduous teeth (SHEDs) induced lipid raft formation in human microglia and that this process was dependent on the milk fat globule-epidermal growth factor-VIII (MFG-E8) /αVβ3/αVβ5 integrins-dependent mechanisms (Jonavice, Romenskaja et al. 2021). We also showed that EVs promoted microglial motility through MFG-E8/P2X4R pathway (Jonavice, Romenskaja et al. 2021). However, it was unclear whether and how the process of EV-induced lipid raft formation is related to TLR4, P2X4R, and integrin αVβ3/αVβ5 signaling pathways.

In the present study, we demonstrate that EVs interfere with TLR4 signaling by suppressing LPS-induced lipid raft formation. We also demonstrate that TLR4, purinergic P2X4R receptor, and integrin αVβ3/αVβ5 signaling pathways are necessary for the EV-mediated induction of lipid rafts.

Our findings could be useful for the development of new therapies targeting disease-associated microglia.

Materials and methods

Explant cultures

For primary explant culture, human oral mucosal stem cells (OMSCs) were isolated from three retromolar explants of a 24-year-old healthy man, under the permission of the Bioethics committee. The biopsy was performed during dental surgery, and the explants were immediately placed in 1 mg/ml glucose DMEM medium containing 10% FBS and a triple dose of antibiotics. Each explant was transferred to a separate well of a 6-well plate, moistened with 100 µl of low glucose DMEM (Biochrom) (1 mg/ml), 10% FBS, and 200 U/ml penicillin, 200 µg/ml streptomycin (all from Biochrom, Berlin, Germany), and stored at 37 ºC in a humidified incubator with 5% CO_2. After adhesion of the explants (approximately 3 to 4 hours), each well was filled with medium. Explants were maintained at 37 ºC in a humidified atmosphere with 5% CO_2, and the medium was routinely changed twice per week. After the appearance of migrating cells, the explants were removed from the wells and the medium changed every three days until the cell cultures reached subconfluence.

Human microglial cell line

The immortalized (SV40) human microglial cell line was acquired from ABM. Human microglial cells were cultured in cell culture flasks coated with 50 µg/ml rat tail collagen I (Gibco) in high glucose DMEM (4.5 mg/ml) supplemented with GlutaMAX (Gibco) and 10% FBS (Biochrom) depleted of extracellular vesicles (EVs).

Isolation of extracellular vesicles

EVs were isolated by differential centrifugation according to Thery et al. with some modifications. All centrifugation steps were performed at 4 ºC. Supernatants from OMSCs cultured in FBS medium depleted of EVs were successively centrifuged at increasing speeds (300 g for 10 minutes, 2000 g for 10 minutes, then 20000 g for 30 minutes). The final supernatants were ultracentrifuged at 100000 g for 70 minutes in a Sorvall LYNX 6000 ultracentrifuge with a T29-8x50 rotor in oak ridge centrifuge tubes with caps (all from Thermo Fisher Scientific, Rochester, NY), then the pellets were resuspended in ice-cold PBS and ultracentrifuged again at 100000 g for 70 minutes at 4ºC. The final pellet of EVs (exosomal fraction) was resuspended in filtered ice-cold PBS and stored at -70 ºC.

Nanoparticle tracking analysis (NTA) was performed using NanoSight LM10 (Malvern Panalytical). The NTA analyses revealed that the EV fractions contained vesicles with a size of approximately 132 nm (Suppl. Fig. 1C). The EV fractions were also positive for the characteristic markers of EVs (HSP70, MFG -E8, CD63) (Suppl. Fig. 1B). The yield of EVs obtained from the supernatants of OMSCs grown to subconfluence on cell culture flasks (with an area of 37.5 cm^2) and conditioned for 72 hours in high-glucose DMEM containing ultracentrifuged EV-depleted FBS medium was defined as one activity unit (1 AU). According to NTA measurements, 1AU of EV contained 3.65×10^8 vesicles.

Lipid raft labeling

Lipid raft labeling was performed with the Vybrant® Alexa Fluor® 594 Lipid Raft Labeling Kit (Thermo Fisher Scientific) according to the manufacturer's protocol with minimal modifications. After all treatments, cells were washed once with complete growth medium and then incubated with 1 µg/ml of fluorescent CT-B (cholera toxin subunit B) for 10 minutes at room temperature. CT-B selectively binds to ganglioside GM1 specifically enriched in the lipid rafts. After washing three times with PBS, the fluorescent CT-B-labeled lipid rafts were cross-linked with the anti-CT-B antibody (200-fold dilution in complete growth medium) for 15 minutes at room temperature. Cells were then washed three times with PBS and fixed in freshly prepared 4% PFA for 20 minutes at room temperature. Cells were washed three times with PBS and mounted on slides with Duolink® PLA mounting medium containing DAPI and analyzed using a Leica TCS SP8 confocal microscope (Leica Microsystems, Mannheim, Germany). Images were acquired with a 63× oil immersion objective. Quantification was performed using Leica Application Suite X (LAS X) software (Leica Microsystems). Mean fluorescence intensity values from each field of view were divided by the number of cells detected (determined by counting DAPI-stained nuclei). Data was collected from three-four biological replicates and quantification was performed in 15-20 fields of view for each experimental group.

Cell treatments in lipid raft labeling experiments

Microglial cells were pre-treated with one of the following agents:

- 5 mM of methyl-β-cyclodextrin (MβCD) (Sigma-Aldrich), lipid raft disrupting agent, for 1 hour;
- 0.5 µg/ml anti-TLR4 blocker antibody (Abcam, HT125) for 4 hours;
- 10 µM 5-BDBD (Tocris Bioscience), P2X4R blocking agent, for 30 min;
- 10 µM of cilengitide (Sigma-Aldrich), an inhibitor of αvβ3/ αvβ5 integrins, for 2 hours.

Cells were then exposed to either EVs (1 AU) or 5 μg/ml of LPS for 30 min, or a combination of both (5 μg/ml of LPS for 15 min and EVs for another 15 min).

Immunocytochemistry

Toll-like receptor 4 labeling was performed by immunocytochemistry. Immediately after treatments with EVs for 2, 6 and 24 hours, cells were fixed in freshly prepared 4% PFA for 20 minutes at room temperature. Then the cells were washed 3 times with PBS and blocked with 1% BSA-PBS solution for 30 min at room temperature. Afterwards, the cells were incubated at 4 °C overnight with the primary antibodies against TLR4 (Novus Biologicals) diluted with a blocking solution in a ratio of 1:200. Next day, the cells were washed 3 times with PBS and incubated with the secondary antibodies conjugated with Alexa Fluor 488 (1:1000, Thermo Fisher Scientific) diluted in PBS at room temperature, in the dark, for 1 hour. Then the cells were washed three times with PBS and mounted on slides with Duolink® PLA mounting medium containing DAPI. Prepared samples were analyzed by Leica TCS SP8 confocal microscope (Leica Microsystems, Mannheim, Germany). Images were acquired with a 63× oil immersion objective. Quantification was performed using Leica Application Suite X (LAS X) software (Leica Microsystems). Mean fluorescence intensity values from each field of view were divided by the number of cells detected (determined by counting DAPI-stained nuclei). Data was collected from three biological replicates and quantification was performed in at least 15 fields of view for each experimental group.

Transmission electron microscopy

TEM of EVs was performed according to the previously reported protocol (Thery, Amigorena et al. 2006) with some modifications. Briefly, EVs in PBS were fixed in 2% paraformaldehyde (PFA) for 40 min on ice. Formvar-carbon-coated copper grids were floated on a 10-μl drop of the fixed EV suspension for 20 minutes at room temperature. Then the grids were washed with PBS and floated on a 30-μl drop of 1% glutaraldehyde solution for 5 minutes at room temperature. They were then washed again eight times by transferring from one drop of distilled water to another. Samples were contrasted on 30 μL drops of 2% neutral uranyl acetate for 5 min at room temperature in the dark. Finally, the grids were air-dried for 5 min. All incubations were displayed on a Parafilm sheet with the coated sides of grids facing to the drop. Samples were analyzed using a transmission electron microscope FEI Morgagni 268.

Protein isolation and western blot analysis

For total cell lysate preparation, cell monolayers were washed three times with cold PBS, pH 7.3, and lysed in Pierce RIPA buffer supplemented with 1× Halt protease inhibitor cocktail for 15 minutes on ice. Cells were scraped off, and lysates were transferred to eppendorfs for 10 minutes. Samples were centrifuged at 18000 g for 20 minutes at 4ºC. After centrifugation, the supernatants were transferred to the new 1.5 ml tubes. For protein isolation from the EVs, we used precipitation with cold acetone. Briefly, four volumes of (-20°C) acetone were added to the EV suspension, mixed, and incubated overnight at -20°C. The next day, after centrifugation (20000 g for 15 minutes at 4ºC), pellets were washed three times with 80 % acetone using the same conditions. Protein concentrations were measured using the NanoPhotometer Pearl (Implen, Munchen, Germany). For Western blot analysis, cell lysates diluted in Laemmli sample buffer were heated at 95 ºC for 5 minutes.
Denatured proteins were separated by sodium dodecyl sulfate-polyacrylamide gel electrophoresis (SDS-PAGE) and blotted onto a PVDF membrane in a semidry Trans-Blot Turbo transfer system (Bio-Rad). Membranes were blocked for 1 hour at room temperature with 5% BSA in PBS containing 0.18% Tween-20 (PBS-Tw). Membranes were then probed overnight at 4°C with primary antibodies against HSP70 (BD Biosciences), CD63, and MFG-E8 (both from Santa Cruz Biotechnology).
After washing three times in PBS-Tw, the membranes were incubated with horseradish peroxidase (HRP)-conjugated secondary antibody (Thermo Fisher Scientific) for 1 h at room temperature. The washing procedure was repeated, and immunoreactive bands were detected with Clarity ECL Western blotting substrate (Bio-Rad) using the ChemiDoc MP system (Bio-Rad).

Evaluation of the phagocytic activity of human microglial cells

Microglial cells were plated on glass coverslips and pre-treated with 10 μM 5-BDBD (Tocris) for 30 min or 4 hours with 0.5 μg/ml anti-TLR4 antibody (Abcam, HT125). Afterwards, cells were treated with EVs (1 AU) and 2 μl/ml of latex beads (L3030, Sigma-Aldrich-Merck) for 6 hours. Digital images of randomly selected fields were acquired with a confocal microscope (Leica SP8, Leica Microsystems), and phagocytic activity was calculated according to the following formula: number of microglial cells containing engulfed latex beads /total number of cells counted × 100. Internalization of phagocytosed material was verified using Z-stacks acquired by confocal microscopy.

Statistical analysis

Statistical analysis was performed using data from at least three independent biological experiments. Plots show the mean and standard error of the mean (SEM). Differences between the groups were compared by the one-way ANOVA following Sidak's post-hoc test. Data that failed the Shapiro-Wilk normality test were analyzed with non-parametric one-way ANOVA (Kruskal-Wallis one-way analysis of variance) following Dunn's post-hoc test. All results were considered significant when $p < 0,05$. Data was analyzed using Graph Pad Prism® 8.0.1 version software (Graph Pad Software, Inc., San Diego, CA, USA).

Results

EVs increase lipid raft formation in human microglia

We first tested how EVs derived from the OMSCs affect lipid raft formation in human microglia cells. Fluorescent cholera toxin subunit B conjugates were used for the specific labeling of ganglioside GM1 which is specifically enriched in the lipid rafts (see Materials and methods section). Microglial cultures were subjected to the following treatments: (1) 1 AU of EVs for 30 min; (2) 5 μg/ml of LPS for 30 min; (3) 5 μg/ml of LPS for 15 min, then 1 AU of EVs for 15 min (Fig 1 A, C).

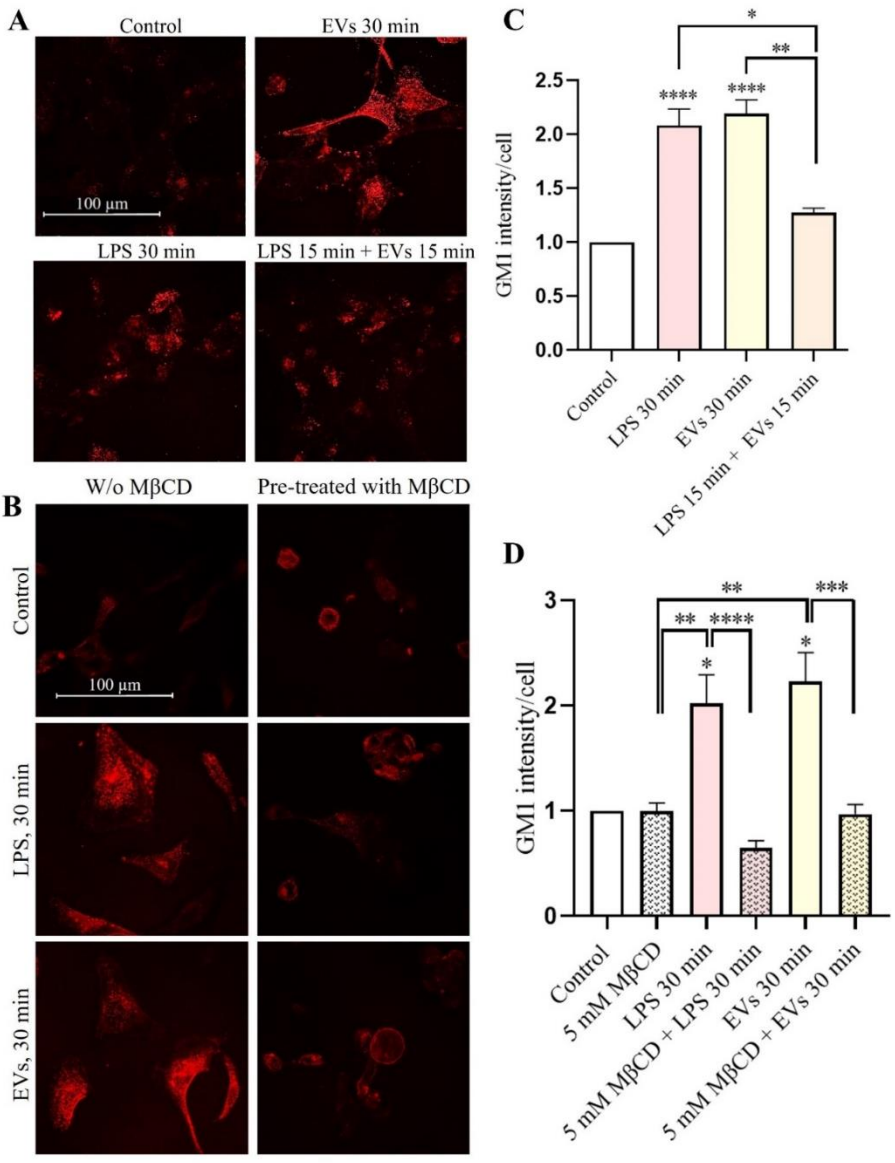

Figure 1. The effects of EVs and LPS on the formation of lipid rafts in human microglia cells. A – Confocal images of labeled lipid rafts (red) in microglia cells. The cells were treated with either EVs (1 AU) or LPS (5 µg/ml) or both for 30 min before lipid raft labeling and fixation. Lipid rafts were labeled in living cells using Vybrant® Alexa Fluor® 594 Lipid Raft Labeling Kit (Thermo Fisher Scientific) according to the manufacturer's protocol (scale bar = 100 µm, magnification – 63x); **B** – Confocal images of labeled lipid rafts (red) in microglia cells pre-treated with 5 mM MβCD for 1 hour (scale bar = 100 µm, magnification – 63x); **C, D** – The mean fluorescence intensity of ganglioside GM1 per cell were measured with Leica Application Suite X (LAS X) software. Data shown represent the results of 15 fields of view for each experimental group from three independent biological experiments (n = 3), plotted as the mean ± SEM, results normalized to control. Statistical significance was analyzed by Kruskal–Wallis test followed by Dunn's post-hoc test in GraphPad Prism 8.0.1 software, * $p<0,05$; ** $p<0,01$; *** $p<0,001$; **** $p < 0,0001$.

Our results show that both EVs and LPS significantly, by more than 2 times increased lipid raft formation in human microglia ($n = 3$, $p < 0.0001$; Fig. 1 A, C). Importantly, combined treatment with LPS and EVs significantly decreased lipid raft formation (compared to the treatment with LPS – by 39 %, and with EVs – by 42 %) (Fig. 1 A, C). This finding indicates possible interference of EVs with the process of LPS-induced lipid raft formation.

As expected, pre-treatment of cells with cholesterol removing agent methyl-β-cyclodextrin (MβCD) for 1 hour inhibited EV- and LPS-induced lipid raft formation in microglia ($n = 3$, in case of treatment with LPS: $p < 0.0001$, with EVs: $p = 0.0005$; Fig. 1 B, D).

Blockage of TLR4 prevents EV-induced lipid raft formation and phagocytosis

Our finding that combined treatment of EVs and LPS inhibited lipid raft formation indicates possible cross-talk between these signaling pathways. We, therefore, tested how blockage of TLR4 with anti-TLR4 antibody (HTA125, Abcam) affects EV-induced lipid raft formation in microglia.

As expected, pre-treatment with blocking antibody for 4 hours significantly decreased LPS-induced lipid raft formation (by 54 %, $n = 3$, $p = 0.0012$; Fig. 2).

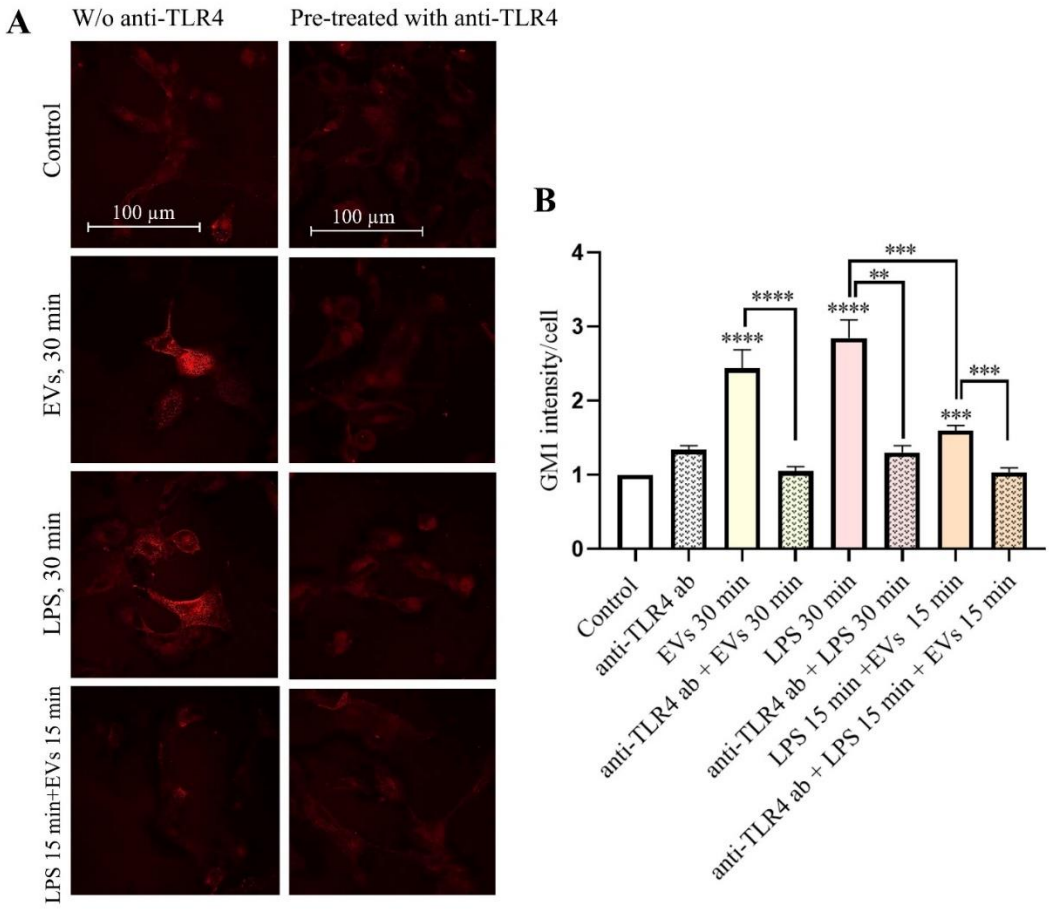

Figure 2. Lipid raft formation after TLR4 receptor inhibition. A – Confocal images of labeled lipid rafts (red) in microglia cells in the presence and absence of pre-treatment with 0.5 µg/ml anti-TLR4 for 4 hours (63× magnification immersion objective, scale bar = 100 µm); **B** – The mean fluorescence intensity of ganglioside GM1 per cell were measured with Leica Application Suite X (LAS X) software, data shown represent the results of 15 fields of view for each experimental group from three independent biological experiments (n = 3), plotted as the mean ± SEM, results normalized to control. Statistical significance was analyzed by Kruskal–Wallis test followed by Dunn's post-hoc test in GraphPad Prism 8.0.1 software, ** $p < 0.01$; *** $p < 0.001$; **** $p < 0.0001$.

Importantly, pre-treatment with anti-TLR4 antibody completely suppressed EV-induced lipid raft formation (by 57 %, n = 3, $p < 0.0001$; Fig. 2) indicating that TLR4 is indispensable for the EVs triggered lipid raft formation in microglia.

We have previously demonstrated that EVs stimulate phagocytosis of human microglia (Jonavice, Tunaitis et al. 2019). We, therefore, tested whether pre-treatment of microglia with anti-TLR4 antibody can affect EV-induced phagocytosis.

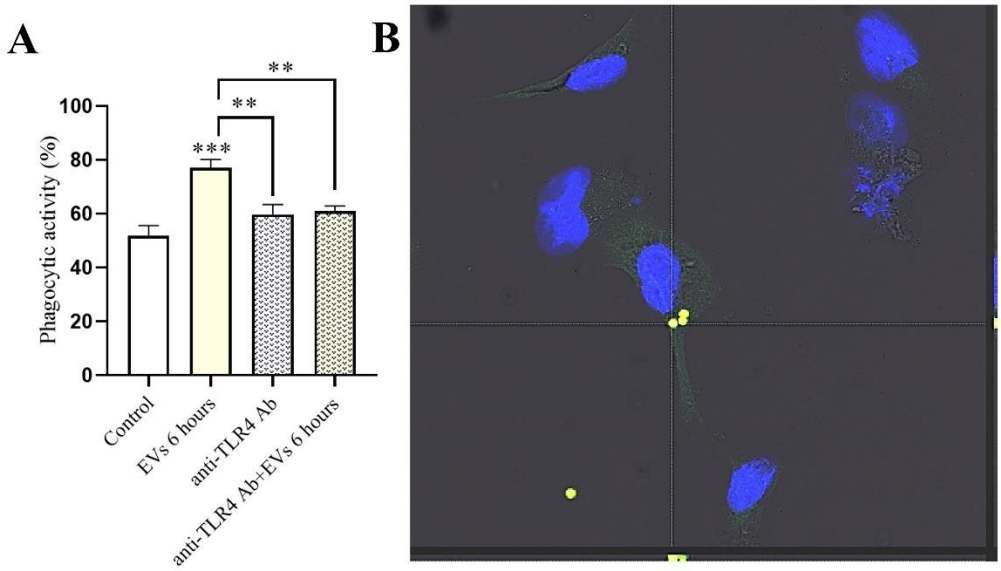

Figure 3. The effects of TLR4 receptor inhibition on the phagocytic activity of microglial cells. **A** – Microglial cells were plated on glass coverslips and pre-treated with 0.5 µg/ml of anti-TLR4 antibody (Abcam, HT125) for 4 hours, then cells were treated with EVs (1 AU) and 2 µl/ml of latex beads (Sigma-Aldrich-Merck) for 6 hours. Phagocytic activity was calculated according to the following formula: number of microglial cells containing engulfed latex beads /total number of cells counted × 100. Data represent mean ± SEM values. Groups were compared with a one-way analysis of variance followed by Sidak's post- hoc test (GraphPad Prism Software). ***$p < 0.001$, **$p < 0.01$. **B** – a representative digital image of randomly selected field acquired with a confocal microscope (Leica SP8, Leica Microsystems). Internalization of phagocytosed material was verified by using Z stacks acquired through confocal microscopy.

The pre-treatment with anti-TLR4 antibody suppressed the EV-induced increase of phagocytic activity to the basal levels ($n = 3$, $p = 0.0089$; Fig. 3A). Our results demonstrate the importance of TLR4 signaling for EV-induced raft formation and phagocytosis in human microglia.

Inhibition of P2X4R prevents EV-induced lipid raft formation and phagocytosis

We have recently demonstrated the importance of purinergic receptor P2X4R signaling for EV-induced microglial migration (Jonavice, Romenskaja et al. 2021). Purinergic receptors are also enriched in the

inflammatory lipid rafts (Garcia-Marcos, Dehaye et al. 2009). We, therefore, tested the effects of P2X4R inhibition on the EV-induced lipid raft formation and phagocytic activity of microglia. We found that pre-treatment with potent selective P2X4R antagonist 5-BDBD suppressed EV-induced lipid raft formation in microglia (by 58 %, n = 4, p = 0.0082; Fig. 4 A, B). Furthermore, blockage of P2X4R also inhibited LPS-induced lipid raft formation (by 65 %, n = 4, p = 0.0017; Fig. 4 B). These findings suggest that the P2X4R pathway may play a universal regulatory role during the initiation of lipid raft formation in human microglia.

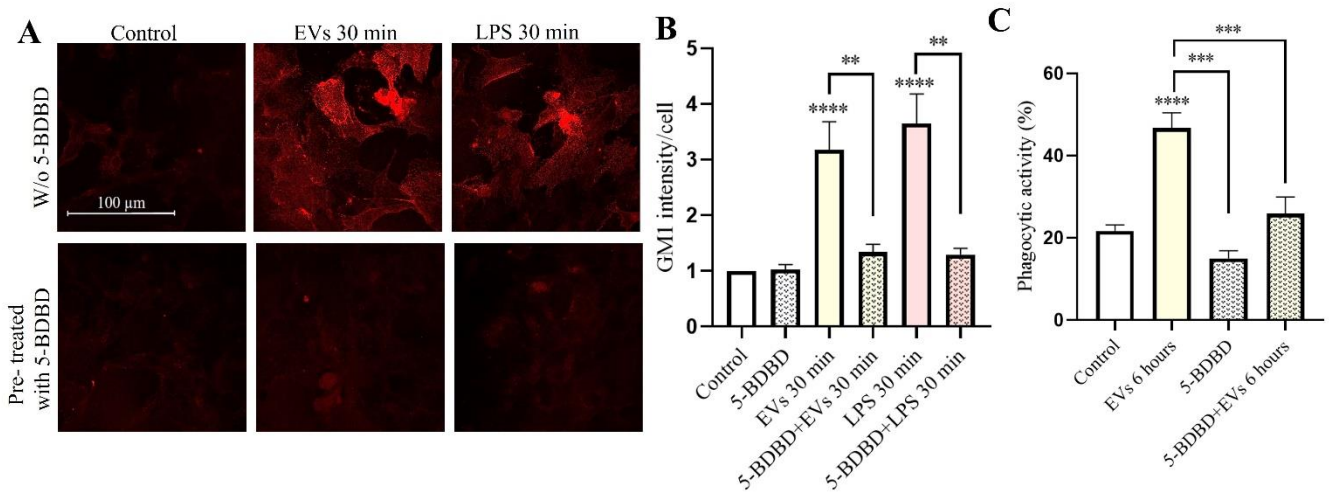

Figure 4. The effects of P2X4R blocking on EV-induced lipid raft formation and phagocytosis. A – Confocal images of labeled lipid rafts (red) in human microglia cells pre-incubated or not with selective P2X4R antagonist 5-BDBD. Images were taken with a Leica SP8 confocal microscope, 63× magnification immersion objective (scale bar - 100 µm). **B –** The mean fluorescence intensity of labeled ganglioside GM1 per cell was measured with Leica Application Suite X (LAS X) software. Data shown represent the results of 20 fields of view for each experimental group from four independent biological experiments (n = 4), plotted as the mean ± SEM, results normalized to control. Statistical significance was analyzed by Kruskal–Wallis test followed by Dunn's post-hoc test in GraphPad Prism 8.0.1 software, ** p<0,01; **** p < 0,0001; **C –** Phagocytic activity was calculated according to the following formula: number of microglial cells containing engulfed latex beads/total number of counted cells × 100. Data represent mean ± SEM values. Groups were compared with a one-way analysis of variance followed by Sidak's post-hoc test (GraphPad Prism Software). ***p < 0.001.

We next tested the effects of selective P2X4R inhibition on the EV-induced phagocytic activity. Blockage of P2X4R with 5-BDBD significantly (by 21 % n =3, p = 0.0005; Figure 4 C) decreased phagocytic capacity of microglial cells.

Inhibition of αvβ3/ αvβ5 integrins with cilengitide suppressed EV- and LPS-induced lipid raft formation in microglia

We detected levels of the MFG-E8 protein in the EV preparations derived from the OMSCs (Suppl Fig. 1C). MFG-E8 protein through its N-terminus Arg-Gly-Asp (RGD) motif binds to αvβ3 integrin receptors on the target cells (Cheyuo, Aziz et al. 2019). We, therefore, tested how blocking αvβ3 and αvβ5 integrins with inhibitor cilengitide affects LPS- and EV-induced lipid raft formation in human microglial cells.

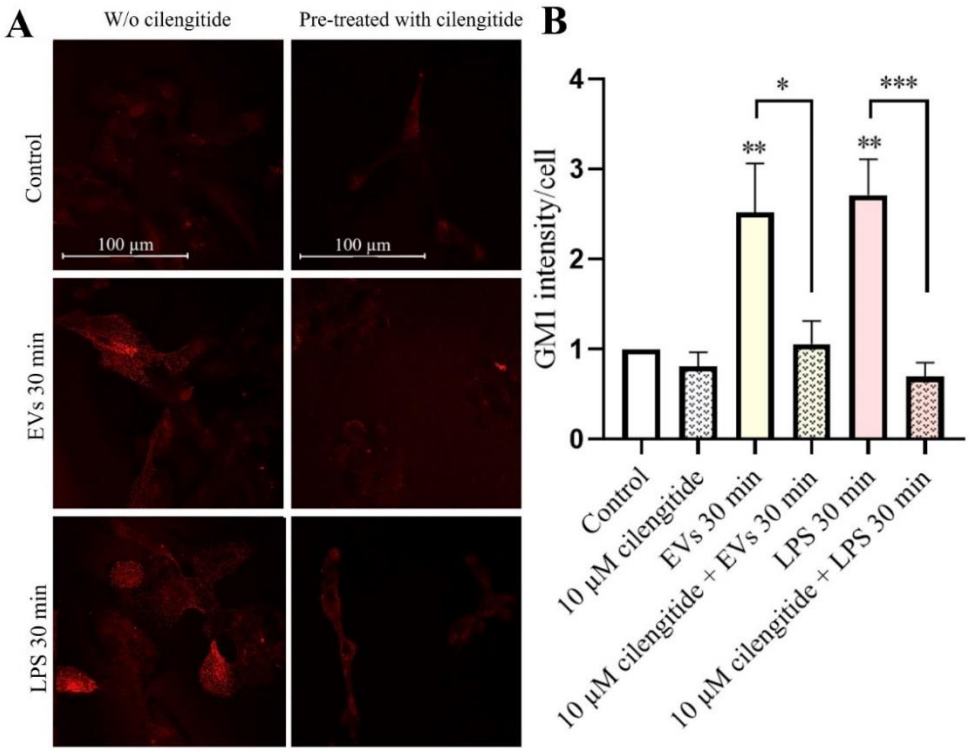

Figure 5. The effects of αvβ3/ αvβ5 integrins inhibition on the EV-induced lipid raft formation in microglia. **A** Confocal images of labeled lipid rafts (red) in human microglia cells pre-incubated or not with selective αvβ3/ αvβ5 integrin antagonist cilengitide (10 µM for 2 hours). Images were taken with a Leica SP8 confocal microscope, 63× magnification immersion objective (scale bar - 100 µm). **B** The mean fluorescence intensity of labeled ganglioside GM1 per cell was measured with Leica Application Suite X (LAS X) software. Data shown represent the results of 20 fields of view for each experimental group from three independent biological experiments (n = 3), plotted as the mean ± SEM, results normalized to control. Statistical significance was analyzed by Kruskal–Wallis test followed by Dunn's post-hoc test in GraphPad Prism 8.0.1 software, * $p < 0.05$; ** $p<0,01$; ***$p < 0.001$.

Our results show that pre-treatment with cilengitide suppressed EV-induced lipid raft formation in microglia (by 58 %, n = 3, p = 0.0199; Fig. 5). Furthermore, blockage of αvβ3/ αvβ5 integrins also

decreased LPS-induced lipid raft formation (by 74 %, n = 3, p = 0.0003; Fig. 5 B). This finding indicates that the αvβ3/ αvβ5 integrin signaling pathway is indispensable for EV- and LPS-induced lipid raft formation in microglia.

Discussion

In the present study, we demonstrate that EVs induce lipid raft formation in human microglia through interaction with TLR4, P2X4R, and αVβ3/αVβ5 signaling pathways. We also show that these signaling pathways are functionally interdependent promoters of EV- and LPS- induced lipid raft formation in microglia.

Our results demonstrate that EVs promoted lipid raft formation at similar levels as LPS, whereas combined treatment resulted in the inhibition of lipid raft formation. Furthermore, blockage of TLR4 with anti-TLR4 antibody prevented EV-induced lipid raft formation showing a direct interaction between EVs and TLR4. Several reports demonstrated that EVs may directly or indirectly target TLR4/NFκB signaling pathway (Cebatariuniene, Kriauciunaite et al. 2019, Jonavice, Tunaitis et al. 2019) (Zhang, Yin et al. 2014) (Goloviznina, Verghese et al. 2016). Apart from bacterial pathogen-associated molecular pattern molecules (PAMPS), TLR4s can be activated by various endogenous molecules acting as inducers of sterile inflammation (Molteni, Gemma et al. 2016). EVs can also act as carriers for the endogenous TLR4 ligands such as heat shock protein 70 (HSP70) (Vabulas, Ahmad-Nejad et al. 2002), fibronectin 1 (Zhang, Yin et al. 2014), high-mobility group box 1 (Radnaa, Richardson et al. 2021) and S100 proteins (Prieto, Sotelo et al. 2017). The physiological importance of the EVs as carriers of endogenous TLR4 ligands was elegantly demonstrated in a study showing that EVs (exosomes) mediated sensory hair cell protection in the inner ear (Breglio, May et al. 2020). In response to the heat stress, inner ear tissue released EVs carrying HSP70, which was required for the pro-survival effects. Direct interactions between exosomal HSP70 and hair cell TLR4 have been confirmed by proximity ligation assays (Breglio, May et al. 2020). Of note, EVs used in our study also expressed considerable amounts of HSP70 protein (Suppl. Fig. 1C). Our finding that pre-treatment with anti-TLR4 antibody prevented EV-induced lipid raft formation supports the model according to which EVs specifically interact with microglial TLR4s. We, therefore, conclude that direct EV-TLR4 interaction is responsible for the induction of the lipid rafts and also for the inhibitory effects of EVs on

the LPS-induced lipid raft formation. We propose that EVs compete with LPS for TLR4s and affect assembly of TLR4 multireceptor complexes. This in turn may impair LPS-dependent oligomerization of resident proteins and prevent the formation of large inflammarafts. We have previously demonstrated that EVs activate the phagocytic response in human microglia (Jonavice, Tunaitis et al. 2019). Here we show that blockage of the TLR4 with anti-TLR4 antibody effectively suppressed EV-induced increase of phagocytic activity in microglia. These findings demonstrate that EVs can at least partially activate microglial phagocytosis through TLR4 signaling pathway.

Purinergic signaling plays a crucial role during ATP-induced chemotaxis and phagocytic activity of microglia (Zabala, Vazquez-Villoldo et al. 2018) (Ohsawa, Irino et al. 2007, Kobayakawa, Ohkawa et al. 2019). We have recently showed that EVs promoted the migration of human microglia through the purinergic receptor P2X4 pathway (Jonavice, Romenskaja et al. 2021). The present study demonstrates that P2XR4 signaling is indispensable for the EV-induced lipid raft formation in the microglia. Furthermore, our results show that blockage of P2X4R activity with selective inhibitor 5-BDBD suppressed LPS-induced lipid raft formation. This finding suggests that the P2X4R signaling pathway may operate as a universal mechanism regulating the induction of lipid rafts in response to ~~the~~ different stimuli. How EVs can trigger P2X4R-dependent lipid raft formation in microglia? Purinergic receptors are enriched in the lipid rafts (Garcia-Marcos, Dehaye et al. 2009) and we have recently demonstrated an interaction between EV-associated MFG-E8 and P2X4R in human microglia (Jonavice, Romenskaja et al. 2021). In addition, EVs may promote P2X4R-induced lipid raft formation indirectly. A recent study showed that EV-induced translocation of lysosomal P2XR4 to the cell membranes was required for cell motility and the formation of vascular networks (Palinski, Monti et al. 2021). Here we also show that inhibition of the P2XR4 pathway suppressed EV-induced phagocytosis of microglia. Thus, both TLR4 and P2XR4 signaling pathways promote lipid raft formation and are indispensable for the EV-induced phagocytosis in human microglia.

We have previously demonstrated that EVs derived from SHEDs induced lipid raft formation in human microglia and that this process was dependent on the MFG-E8/integrin αVβ3/αVβ5-dependent mechanisms (Jonavice, Romenskaja et al. 2021). In the present study, we used EVs derived from the OMSCs and obtained very similar results. Of note, EVs from the OMSCs also expressed high levels of MFG-E8 protein (Suppl Fig. 1 C) which is a secretory glycoprotein acting as a molecular bridge connecting phosphatidylserine (PS) exposed on the outer membranes of the EVs with microglial integrin αVβ3/αVβ5 receptors (Cheyuo, Aziz et al. 2019). Inhibition of αVβ3/αVβ5 receptors with

cilengitide suppressed EV-induced lipid raft formation. Moreover, cilengitide also significantly suppressed LPS-induced lipid raft formation in microglia. Thus, similarly to our previous observation with P2X4R, integrin αVβ3/αVβ5 signaling may also operate as a universal mechanism regulating the induction of lipid rafts in response to the different stimuli.

Based on these findings, we propose that EVs carrying MFG-E8 proteins and endogenous TLR4 ligands (HSP70) are recognized by the αVβ3/αVβ5 integrin receptors and TLR4s and also directly or indirectly activate P2X4Rs of microglial cells (Fig. 6).

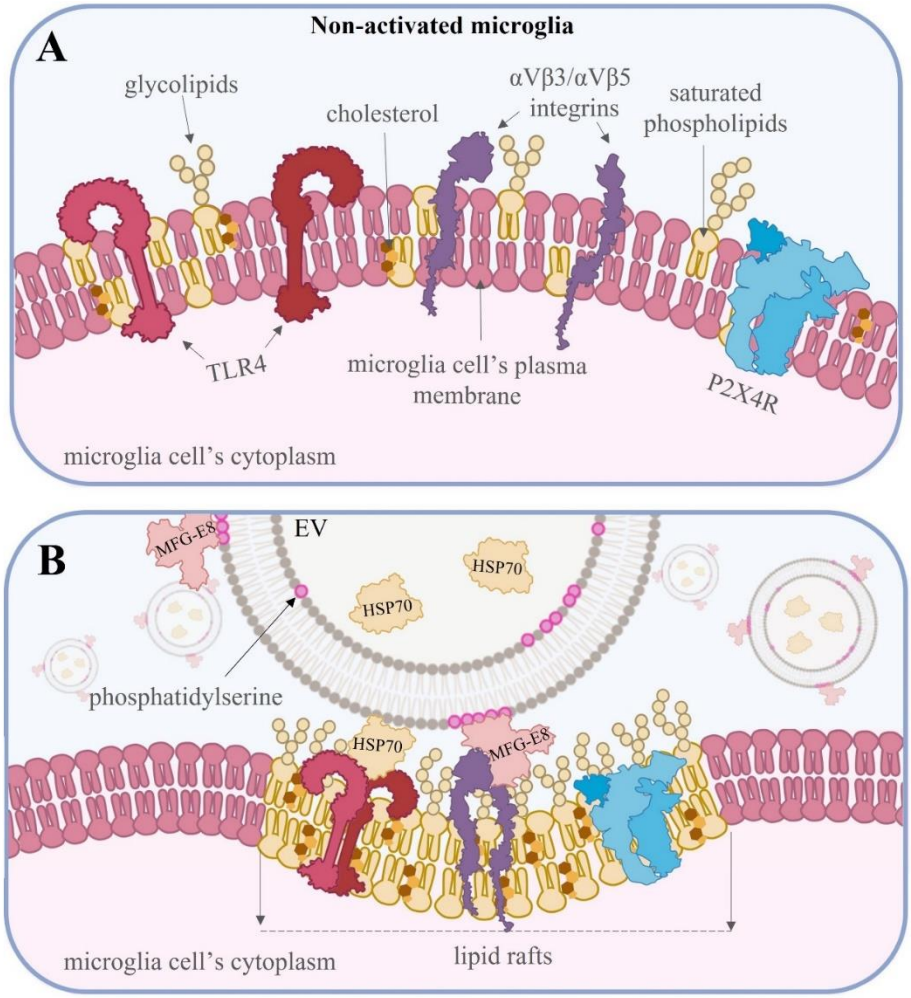

Figure 6. Proposed mechanism for EV action on microglial cells (see text for the explanations).

These events trigger lipid raft formation and enlargement leading to the initiation of various downstream signaling pathways in the microglia. We also propose that TLR4, αVβ3/αVβ5 integrin, and P2X4R comprise a network of functionally interdependent signaling units regulating the induction and enlargement of lipid rafts in response to different stimuli. Further studies are needed to confirm the

presence of similar signaling networks regulating lipid raft formation in other experimental *in vitro* and *in vivo* models.

In conclusion, we demonstrate for the first time that EVs induce lipid raft formation in human microglia through interaction with TLR4, P2X4R, and αVβ3/αVβ5 signaling pathways. Our results provide new insights about the molecular mechanisms regulating EV/microglia interactions that could be helpful for the development of new therapeutic strategies against neurological disorders.

Conflict of interest

There is no conflict of interests to disclose.

Acknowledgements

This project has received funding from European Regional Development Fund (project No 01.2.2-LMT-K-718-01-0012) under grant agreement with the Research Council of Lithuania (LMTLT).

Figure legends

Figure 1. The effects of EVs and LPS on the formation of lipid rafts in human microglia cells. A – Confocal images of labeled lipid rafts (red) in microglia cells. The cells were treated with either EVs (1 AU) or LPS (5 μg/ml) or both for 30 min before lipid raft labeling and fixation. Lipid rafts were labeled in living cells using Vybrant® Alexa Fluor® 594 Lipid Raft Labeling Kit (Thermo Fisher Scientific) according to the manufacturer's protocol (scale bar = 100 μm, magnification – 63x); **B** – Confocal images of labeled lipid rafts (red) in microglia cells pre-treated with 5 mM MβCD for 1 hour (scale bar = 100 μm, magnification – 63x); **C, D** – The mean fluorescence intensity of ganglioside GM1 per cell were measured with Leica Application Suite X (LAS X) software. Data shown represent the results of 15 fields of view for each experimental group from three independent biological experiments (n = 3), plotted as the mean ± SEM, results normalized to control. Statistical significance was analyzed by Kruskal–Wallis test followed by Dunn's post-hoc test in GraphPad Prism 8.0.1 software, * p<0,05; ** p<0,01; *** p<0,001; **** p < 0,0001.

Figure 2. Lipid raft formation after TLR4 receptor inhibition. A – Confocal images of labeled lipid rafts (red) in microglia cells in the presence and absence of pre-treatment with 0.5 μg/ml anti-TLR4 for 4 hours (63× magnification immersion objective, scale bar = 100 μm); **B** – The mean fluorescence intensity of ganglioside GM1 per cell were measured with Leica Application Suite X (LAS X) software, data shown represent the results of 15 fields of view for each experimental group from three independent biological experiments (n = 3), plotted as the mean ± SEM, results normalized to control. Statistical

significance was analyzed by Kruskal–Wallis test followed by Dunn's post-hoc test in GraphPad Prism 8.0.1 software, ** $p < 0.01$; *** $p < 0.001$; **** $p < 0.0001$.

Figure 3. The effects of TLR4 receptor inhibition on the phagocytic activity of microglial cells. **A** – Microglial cells were plated on glass coverslips and pre-treated with 0.5 μg/ml of anti-TLR4 antibody (Abcam, HT125) for 4 hours, then cells were treated with EVs (1 AU) and 2 μl/ml of latex beads (Sigma-Aldrich-Merck) for 6 hours. Phagocytic activity was calculated according to the following formula: number of microglial cells containing engulfed latex beads /total number of cells counted × 100. Data represent mean ± SEM values. Groups were compared with a one-way analysis of variance followed by Sidak's post- hoc test (GraphPad Prism Software). ***$p < 0.001$, **$p < 0.01$. **B** – a representative digital image of randomly selected field acquired with a confocal microscope (Leica SP8, Leica Microsystems). Internalization of phagocytosed material was verified by using Z stacks acquired through confocal microscopy.

Figure 4. The effects of P2X4R blocking on EV-induced lipid raft formation and phagocytosis. A – Confocal images of labeled lipid rafts (red) in human microglia cells pre-incubated or not with selective P2X4R antagonist 5-BDBD. Images were taken with a Leica SP8 confocal microscope, 63× magnification immersion objective (scale bar - 100 μm). **B –** The mean fluorescence intensity of labeled ganglioside GM1 per cell was measured with Leica Application Suite X (LAS X) software. Data shown represent the results of 20 fields of view for each experimental group from four independent biological experiments (n = 4), plotted as the mean ± SEM, results normalized to control. Statistical significance was analyzed by Kruskal–Wallis test followed by Dunn's post-hoc test in GraphPad Prism 8.0.1 software, ** $p<0,01$; **** $p < 0,0001$; **C –** Phagocytic activity was calculated according to the following formula: number of microglial cells containing engulfed latex beads/total number of counted cells × 100. Data represent mean ± SEM values. Groups were compared with a one-way analysis of variance followed by Sidak's post-hoc test (GraphPad Prism Software). ***$p < 0.001$.

Figure 5. The effects of αvβ3/ αvβ5 integrins inhibition on the EV-induced lipid raft formation in microglia. A Confocal images of labeled lipid rafts (red) in human microglia cells pre-incubated or not with selective αvβ3/ αvβ5 integrin antagonist cilengitide (10 μM for 2 hours). Images were taken with a Leica SP8 confocal microscope, 63× magnification immersion objective (scale bar - 100 μm). **B** The mean fluorescence intensity of labeled ganglioside GM1 per cell was measured with Leica Application Suite X (LAS X) software. Data shown represent the results of 20 fields of view for each experimental group from three independent biological experiments (n = 3), plotted as the mean ± SEM, results normalized to control. Statistical significance was analyzed by Kruskal–Wallis test followed by Dunn's post-hoc test in GraphPad Prism 8.0.1 software, * $p < 0.05$; ** $p<0,01$; ***$p < 0.001$.

Figure 6. Proposed mechanism for EV action on microglial cells.

References

Alvarez-Erviti, L., Y. Seow, H. Yin, C. Betts, S. Lakhal and M. J. Wood (2011). "Delivery of siRNA to the mouse brain by systemic injection of targeted exosomes." Nat Biotechnol **29**(4): 341-345.

Augusto-Oliveira, M., G. P. Arrifano, C. I. Delage, M. E. Tremblay, M. E. Crespo-Lopez and A. Verkhratsky (2022). "Plasticity of microglia." Biol Rev Camb Philos Soc **97**(1): 217-250.

Boumechache, M., M. Masin, J. M. Edwardson, D. C. Gorecki and R. Murrell-Lagnado (2009). "Analysis of assembly and trafficking of native P2X4 and P2X7 receptor complexes in rodent immune cells." J Biol Chem **284**(20): 13446-13454.

Breglio, A. M., L. A. May, M. Barzik, N. C. Welsh, S. P. Francis, T. Q. Costain, L. Wang, D. E. Anderson, R. S. Petralia, Y. X. Wang, T. B. Friedman, M. J. Wood and L. L. Cunningham (2020). "Exosomes mediate sensory hair cell protection in the inner ear." J Clin Invest **130**(5): 2657-2672.

Cebatariuniene, A., K. Kriauciunaite, J. Prunskaite, V. Tunaitis and A. Pivoriunas (2019). "Extracellular Vesicles Suppress Basal and Lipopolysaccharide-Induced NFkappaB Activity in Human Periodontal Ligament Stem Cells." Stem Cells Dev **28**(15): 1037-1049.

Cheyuo, C., M. Aziz and P. Wang (2019). "Neurogenesis in Neurodegenerative Diseases: Role of MFG-E8." Front Neurosci **13**: 569.

Garcia-Marcos, M., J. P. Dehaye and A. Marino (2009). "Membrane compartments and purinergic signalling: the role of plasma membrane microdomains in the modulation of P2XR-mediated signalling." FEBS J **276**(2): 330-340.

Goloviznina, N. A., S. C. Verghese, Y. M. Yoon, O. Taratula, D. L. Marks and P. Kurre (2016). "Mesenchymal Stromal Cell-derived Extracellular Vesicles Promote Myeloid-biased Multipotent Hematopoietic Progenitor Expansion via Toll-Like Receptor Engagement." J Biol Chem **291**(47): 24607-24617.

Green, J. M., A. Zheleznyak, J. Chung, F. P. Lindberg, M. Sarfati, W. A. Frazier and E. J. Brown (1999). "Role of cholesterol in formation and function of a signaling complex involving alphavbeta3, integrin-associated protein (CD47), and heterotrimeric G proteins." J Cell Biol **146**(3): 673-682.

Guo, S., N. Perets, O. Betzer, S. Ben-Shaul, A. Sheinin, I. Michaelevski, R. Popovtzer, D. Offen and S. Levenberg (2019). "Intranasal Delivery of Mesenchymal Stem Cell Derived Exosomes Loaded with Phosphatase and Tensin Homolog siRNA Repairs Complete Spinal Cord Injury." ACS Nano **13**(9): 10015-10028.

Herman, S., I. Fishel and D. Offen (2021). "Intranasal delivery of mesenchymal stem cells-derived extracellular vesicles for the treatment of neurological diseases." Stem Cells **39**(12): 1589-1600.

Jarmalaviciute, A. and A. Pivoriunas (2016). "Exosomes as a potential novel therapeutic tools against neurodegenerative diseases." Pharmacol Res **113**(Pt B): 816-822.

Jonavice, U., D. Romenskaja, K. Kriauciunaite, A. Jarmalaviciute, J. Pajarskiene, V. Kaseta, V. Tunaitis, T. Malm, R. Giniatulin and A. Pivoriunas (2021). "Extracellular Vesicles from Human Teeth Stem Cells Trigger ATP Release and Promote Migration of Human Microglia through P2X4 Receptor/MFG-E8-Dependent Mechanisms." Int J Mol Sci **22**(20).

Jonavice, U., V. Tunaitis, K. Kriauciunaite, A. Jarmalaviciute and A. Pivoriunas (2019). "Extracellular vesicles can act as a potent immunomodulators of human microglial cells." J Tissue Eng Regen Med **13**(2): 309-318.

Kobayakawa, K., Y. Ohkawa, S. Yoshizaki, T. Tamaru, T. Saito, K. Kijima, K. Yokota, M. Hara, K. Kubota, Y. Matsumoto, K. Harimaya, K. Ozato, T. Masuda, M. Tsuda, T. Tamura, K. Inoue, V. R. Edgerton, Y. Iwamoto, Y. Nakashima and S. Okada (2019). "Macrophage centripetal migration drives spontaneous healing process after spinal cord injury." Sci Adv **5**(5): eaav5086.

Kopp, R., A. Krautloher, A. Ramirez-Fernandez and A. Nicke (2019). "P2X7 Interactions and Signaling - Making Head or Tail of It." Front Mol Neurosci **12**: 183.
Li, Y., H. Wu, X. Jiang, Y. Dong, J. Zheng and J. Gao (2022). "New idea to promote the clinical applications of stem cells or their extracellular vesicles in central nervous system disorders: Combining with intranasal delivery." Acta Pharm Sin B **12**(8): 3215-3232.
Lietha, D. and T. Izard (2020). "Roles of Membrane Domains in Integrin-Mediated Cell Adhesion." Int J Mol Sci **21**(15).
Long, Q., D. Upadhya, B. Hattiangady, D. K. Kim, S. Y. An, B. Shuai, D. J. Prockop and A. K. Shetty (2017). "Intranasal MSC-derived A1-exosomes ease inflammation, and prevent abnormal neurogenesis and memory dysfunction after status epilepticus." Proc Natl Acad Sci U S A **114**(17): E3536-E3545.
Losurdo, M., M. Pedrazzoli, C. D'Agostino, C. A. Elia, F. Massenzio, E. Lonati, M. Mauri, L. Rizzi, L. Molteni, E. Bresciani, E. Dander, G. D'Amico, A. Bulbarelli, A. Torsello, M. Matteoli, M. Buffelli and S. Coco (2020). "Intranasal delivery of mesenchymal stem cell-derived extracellular vesicles exerts immunomodulatory and neuroprotective effects in a 3xTg model of Alzheimer's disease." Stem Cells Transl Med **9**(9): 1068-1084.
Miller, Y. I., J. M. Navia-Pelaez, M. Corr and T. L. Yaksh (2020). "Lipid rafts in glial cells: role in neuroinflammation and pain processing." J Lipid Res **61**(5): 655-666.
Molteni, M., S. Gemma and C. Rossetti (2016). "The Role of Toll-Like Receptor 4 in Infectious and Noninfectious Inflammation." Mediators Inflamm **2016**: 6978936.
Narbute, K., V. Pilipenko, J. Pupure, Z. Dzirkale, U. Jonavice, V. Tunaitis, K. Kriauciunaite, A. Jarmalaviciute, B. Jansone, V. Klusa and A. Pivoriunas (2019). "Intranasal Administration of Extracellular Vesicles Derived from Human Teeth Stem Cells Improves Motor Symptoms and Normalizes Tyrosine Hydroxylase Expression in the Substantia Nigra and Striatum of the 6-Hydroxydopamine-Treated Rats." Stem Cells Transl Med **8**(5): 490-499.
Ohsawa, K., Y. Irino, Y. Nakamura, C. Akazawa, K. Inoue and S. Kohsaka (2007). "Involvement of P2X4 and P2Y12 receptors in ATP-induced microglial chemotaxis." Glia **55**(6): 604-616.
Palinski, W., M. Monti, R. Camerlingo, I. Iacobucci, S. Bocella, F. Pinto, C. Iannuzzi, G. Mansueto, S. Pignatiello, F. Fazioli, M. Gallo, L. Marra, F. Cozzolino, A. De Chiara, P. Pucci, A. Bilancio and F. de Nigris (2021). "Lysosome purinergic receptor P2X4 regulates neoangiogenesis induced by microvesicles from sarcoma patients." Cell Death Dis **12**(9): 797.
Perets, N., O. Betzer, R. Shapira, S. Brenstein, A. Angel, T. Sadan, U. Ashery, R. Popovtzer and D. Offen (2019). "Golden Exosomes Selectively Target Brain Pathologies in Neurodegenerative and Neurodevelopmental Disorders." Nano Lett **19**(6): 3422-3431.
Plociennikowska, A., A. Hromada-Judycka, K. Borzecka and K. Kwiatkowska (2015). "Co-operation of TLR4 and raft proteins in LPS-induced pro-inflammatory signaling." Cell Mol Life Sci **72**(3): 557-581.
Prieto, D., N. Sotelo, N. Seija, S. Sernbo, C. Abreu, R. Duran, M. Gil, E. Sicco, V. Irigoin, C. Oliver, A. I. Landoni, R. Gabus, G. Dighiero and P. Oppezzo (2017). "S100-A9 protein in exosomes from chronic lymphocytic leukemia cells promotes NF-kappaB activity during disease progression." Blood **130**(6): 777-788.
Radnaa, E., L. S. Richardson, S. Sheller-Miller, T. Baljinnyam, M. de Castro Silva, A. Kumar Kammala, R. Urrabaz-Garza, T. Kechichian, S. Kim, A. Han and R. Menon (2021). "Extracellular vesicle mediated feto-maternal HMGB1 signaling induces preterm birth." Lab Chip **21**(10): 1956-1973.
Ransohoff, R. M. (2016). "How neuroinflammation contributes to neurodegeneration." Science **353**(6301): 777-783.
Sezgin, E., I. Levental, S. Mayor and C. Eggeling (2017). "The mystery of membrane organization: composition, regulation and roles of lipid rafts." Nat Rev Mol Cell Biol **18**(6): 361-374.

Song, W. M. and M. Colonna (2018). "The identity and function of microglia in neurodegeneration." Nat Immunol **19**(10): 1048-1058.
Suurvali, J., P. Boudinot, J. Kanellopoulos and S. Ruutel Boudinot (2017). "P2X4: A fast and sensitive purinergic receptor." Biomed J **40**(5): 245-256.
Sviridov, D., N. Mukhamedova and Y. I. Miller (2020). "Lipid rafts as a therapeutic target." J Lipid Res **61**(5): 687-695.
Thery, C., S. Amigorena, G. Raposo and A. Clayton (2006). "Isolation and characterization of exosomes from cell culture supernatants and biological fluids." Curr Protoc Cell Biol **Chapter 3**: Unit 3 22.
Ulmann, L., J. P. Hatcher, J. P. Hughes, S. Chaumont, P. J. Green, F. Conquet, G. N. Buell, A. J. Reeve, I. P. Chessell and F. Rassendren (2008). "Up-regulation of P2X4 receptors in spinal microglia after peripheral nerve injury mediates BDNF release and neuropathic pain." J Neurosci **28**(44): 11263-11268.
Vabulas, R. M., P. Ahmad-Nejad, S. Ghose, C. J. Kirschning, R. D. Issels and H. Wagner (2002). "HSP70 as endogenous stimulus of the Toll/interleukin-1 receptor signal pathway." J Biol Chem **277**(17): 15107-15112.
Wiklander, O. P. B., M. A. Brennan, J. Lotvall, X. O. Breakefield and S. El Andaloussi (2019). "Advances in therapeutic applications of extracellular vesicles." Sci Transl Med **11**(492).
Woller, S. A., S. H. Choi, E. J. An, H. Low, D. A. Schneider, R. Ramachandran, J. Kim, Y. S. Bae, D. Sviridov, M. Corr, T. L. Yaksh and Y. I. Miller (2018). "Inhibition of Neuroinflammation by AIBP: Spinal Effects upon Facilitated Pain States." Cell Rep **23**(9): 2667-2677.
Zabala, A., N. Vazquez-Villoldo, B. Rissiek, J. Gejo, A. Martin, A. Palomino, A. Perez-Samartin, K. R. Pulagam, M. Lukowiak, E. Capetillo-Zarate, J. Llop, T. Magnus, F. Koch-Nolte, F. Rassendren, C. Matute and M. Domercq (2018). "P2X4 receptor controls microglia activation and favors remyelination in autoimmune encephalitis." EMBO Mol Med **10**(8).
Zhang, B., Y. Yin, R. C. Lai, S. S. Tan, A. B. Choo and S. K. Lim (2014). "Mesenchymal stem cells secrete immunologically active exosomes." Stem Cells Dev **23**(11): 1233-1244.

Figures

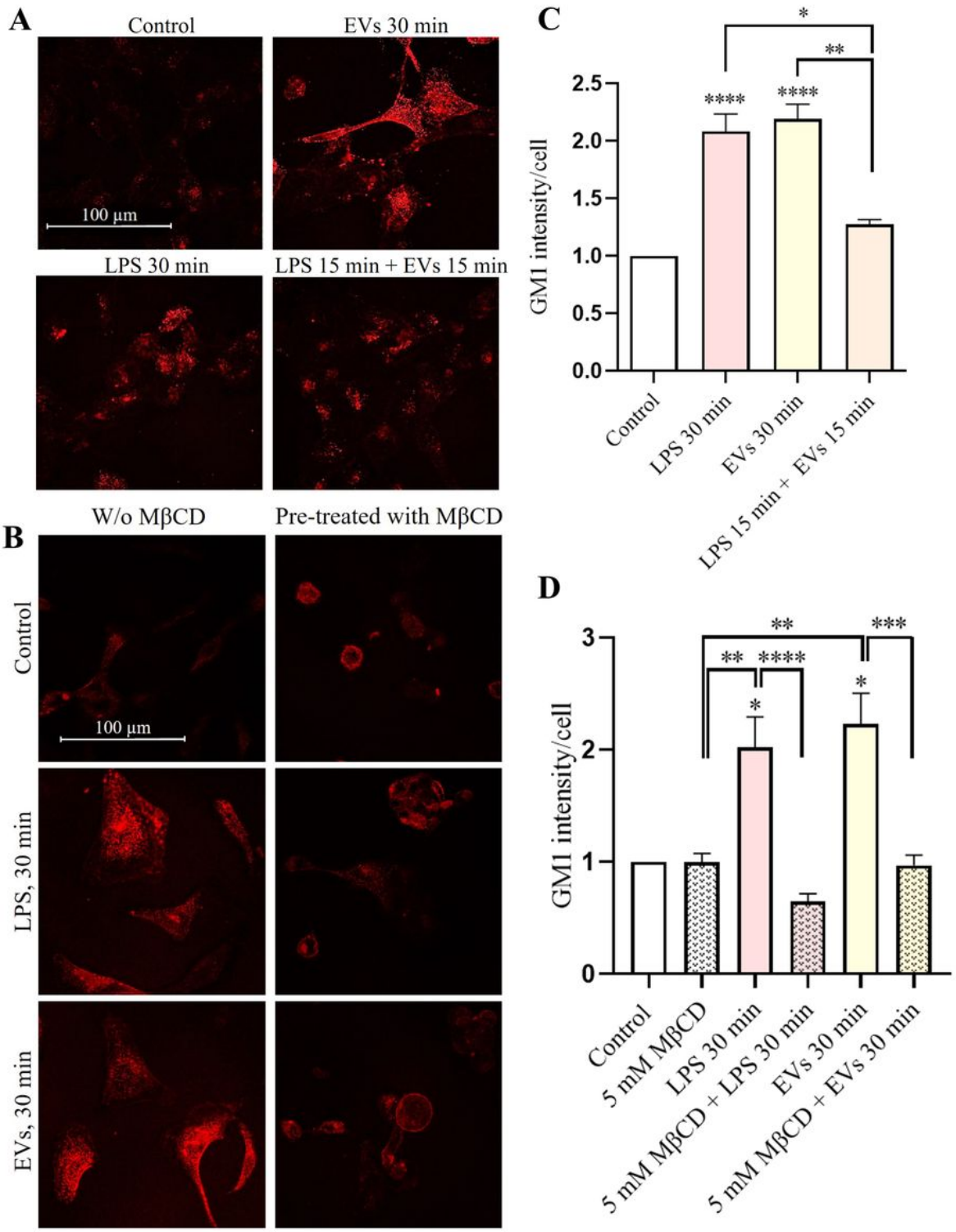

Figure 1

The effects of EVs and LPS on the formation of lipid rafts in human microglia cells. A – Confocal images of labeled lipid rafts (red) in microglia cells. The cells were treated with either EVs (1 AU) or LPS (5 µg/ml) or both for 30 min before lipid raft labeling and fixation. Lipid rafts were labeled in living cells using

Vybrant® Alexa Fluor® 594 Lipid Raft Labeling Kit (Thermo Fisher Scientific) according to the manufacturer's protocol (scale bar = 100 μm, magnification – 63x); **B** – Confocal images of labeled lipid rafts (red) in microglia cells pre-treated with 5 mM MβCD for 1 hour (scale bar = 100 μm, magnification – 63x); **C, D** – The mean fluorescence intensity of ganglioside GM1 per cell were measured with Leica Application Suite X (LAS X) software. Data shown represent the results of 15 fields of view for each experimental group from three independent biological experiments (n = 3), plotted as the mean ± SEM, results normalized to control. Statistical significance was analyzed by Kruskal–Wallis test followed by Dunn's post-hoc test in GraphPad Prism 8.0.1 software, * p<0,05; ** p<0,01; *** p<0,001; **** p < 0,0001.

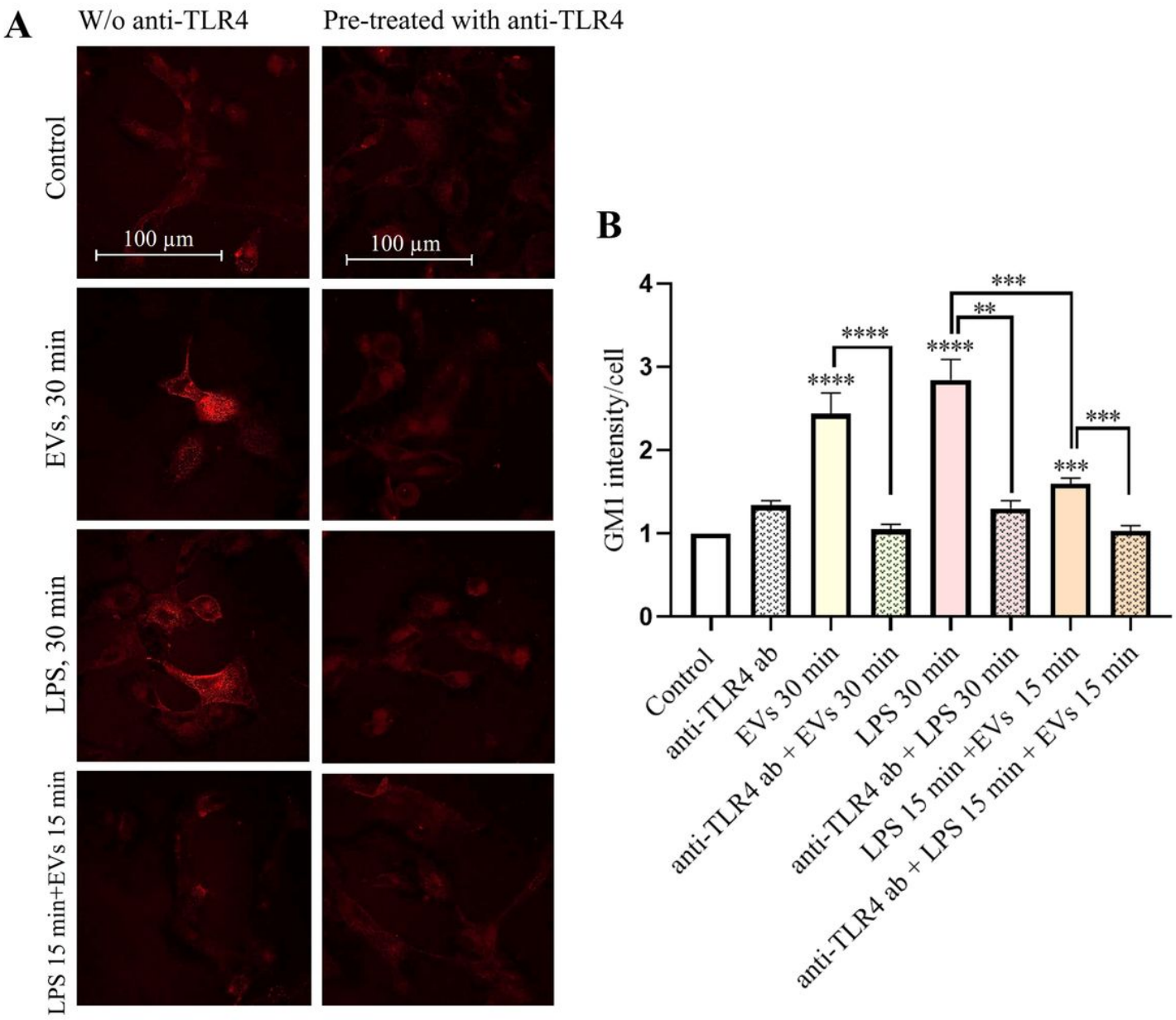

Figure 2

Lipid raft formation after TLR4 receptor inhibition. A – Confocal images of labeled lipid rafts (red) in microglia cells in the presence and absence of pre-treatment with 0.5 μg/ml anti-TLR4 for 4 hours (63× magnification immersion objective, scale bar = 100 μm); **B** – The mean fluorescence intensity of ganglioside GM1 per cell were measured with Leica Application Suite X (LAS X) software, data shown represent the results of 15 fields of view for each experimental group from three independent biological experiments (n = 3), plotted as the mean ± SEM, results normalized to control. Statistical significance was analyzed by Kruskal–Wallis test followed by Dunn's post-hoc test in GraphPad Prism 8.0.1 software, ** $p < 0.01$; *** $p < 0.001$; **** $p < 0.0001$.

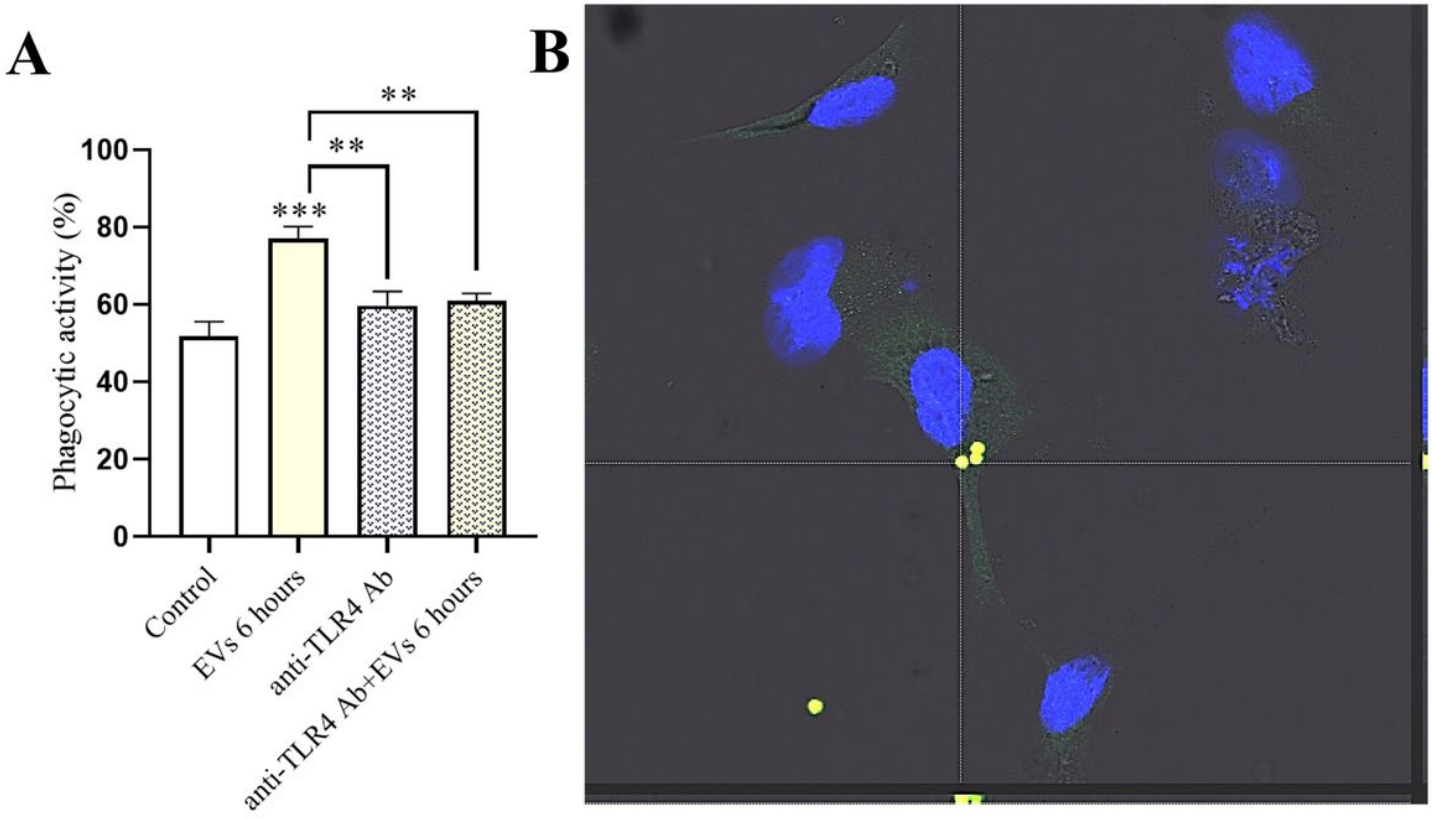

Figure 3

The effects of TLR4 receptor inhibition on the phagocytic activity of microglial cells. **A**– Microglial cells were plated on glass coverslips and pre-treated with 0.5 μg/ml of anti-TLR4 antibody (Abcam, HT125) for 4 hours, then cells were treated with EVs (1 AU) and 2 μl/ml of latex beads (Sigma-Aldrich-Merck) for 6 hours. Phagocytic activity was calculated according to the following formula: number of microglial cells containing engulfed latex beads /total number of cells counted × 100. Data represent mean ± SEM values. Groups were compared with a one way analysis of variance followed by Sidak's post hoc test (GraphPad Prism Software). ***$p < 0.001$, **$p < 0.01$. **B** – a representative digital image of randomly selected field acquired with a confocal microscope (Leica SP8, Leica Microsystems). Internalization of phagocytosed material was verified by using Z stacks acquired through confocal microscopy.

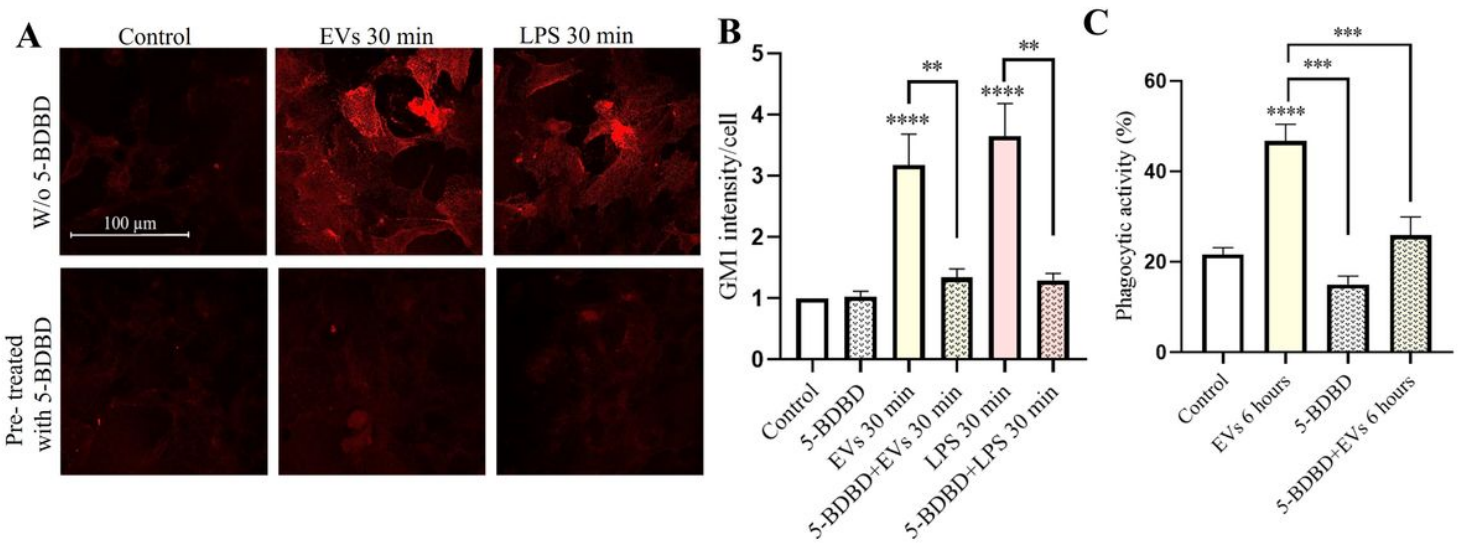

Figure 4

The effects of P2X4R blocking on EV-induced lipid raft formation and phagocytosis. A – Confocal images of labeled lipid rafts (red) in human microglia cells pre-incubated or not with selective P2X4R antagonist 5-BDBD. Images were taken with a Leica SP8 confocal microscope, 63× magnification immersion objective (scale bar - 100 µm). **B –** The mean fluorescence intensity of labeled ganglioside GM1 per cell was measured with Leica Application Suite X (LAS X) software. Data shown represent the results of 20 fields of view for each experimental group from four independent biological experiments (n = 4), plotted as the mean ± SEM, results normalized to control. Statistical significance was analyzed by Kruskal–Wallis test followed by Dunn's post-hoc test in GraphPad Prism 8.0.1 software, ** p<0,01; **** p < 0,0001; **C –** Phagocytic activity was calculated according to the following formula: number of microglial cells containing engulfed latex beads/total number of counted cells × 100. Data represent mean ± SEM values. Groups were compared with a one way analysis of variance followed by Sidak's post hoc test (GraphPad Prism Software). ***p < 0.001.

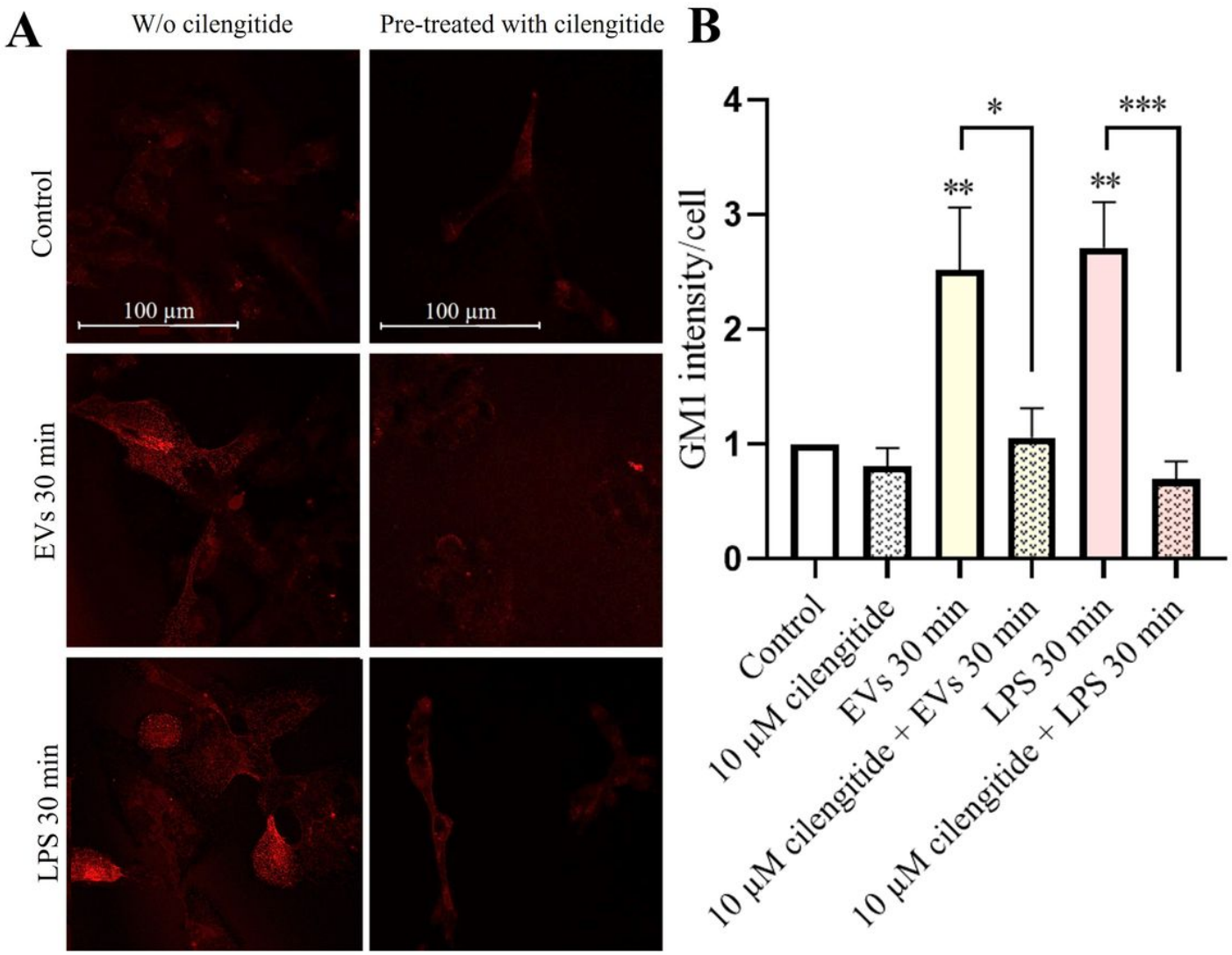

Figure 5

The effects of αvβ3/ αvβ5 integrins inhibition on the EV-induced lipid raft formation in microglia. A Confocal images of labeled lipid rafts (red) in human microglia cells pre-incubated or not with selective αvβ3/ αvβ5 integrin antagonist cilengitide (10 µM for 2 hours). Images were taken with a Leica SP8 confocal microscope, 63× magnification immersion objective (scale bar - 100 µm). **B** The mean fluorescence intensity of labeled ganglioside GM1 per cell was measured with Leica Application Suite X (LAS X) software. Data shown represent the results of 20 fields of view for each experimental group from three independent biological experiments (n = 3), plotted as the mean ± SEM, results normalized to control. Statistical significance was analyzed by Kruskal–Wallis test followed by Dunn's post-hoc test in GraphPad Prism 8.0.1 software, * $p < 0.05$; ** $p<0,01$; ***$p < 0.001$.

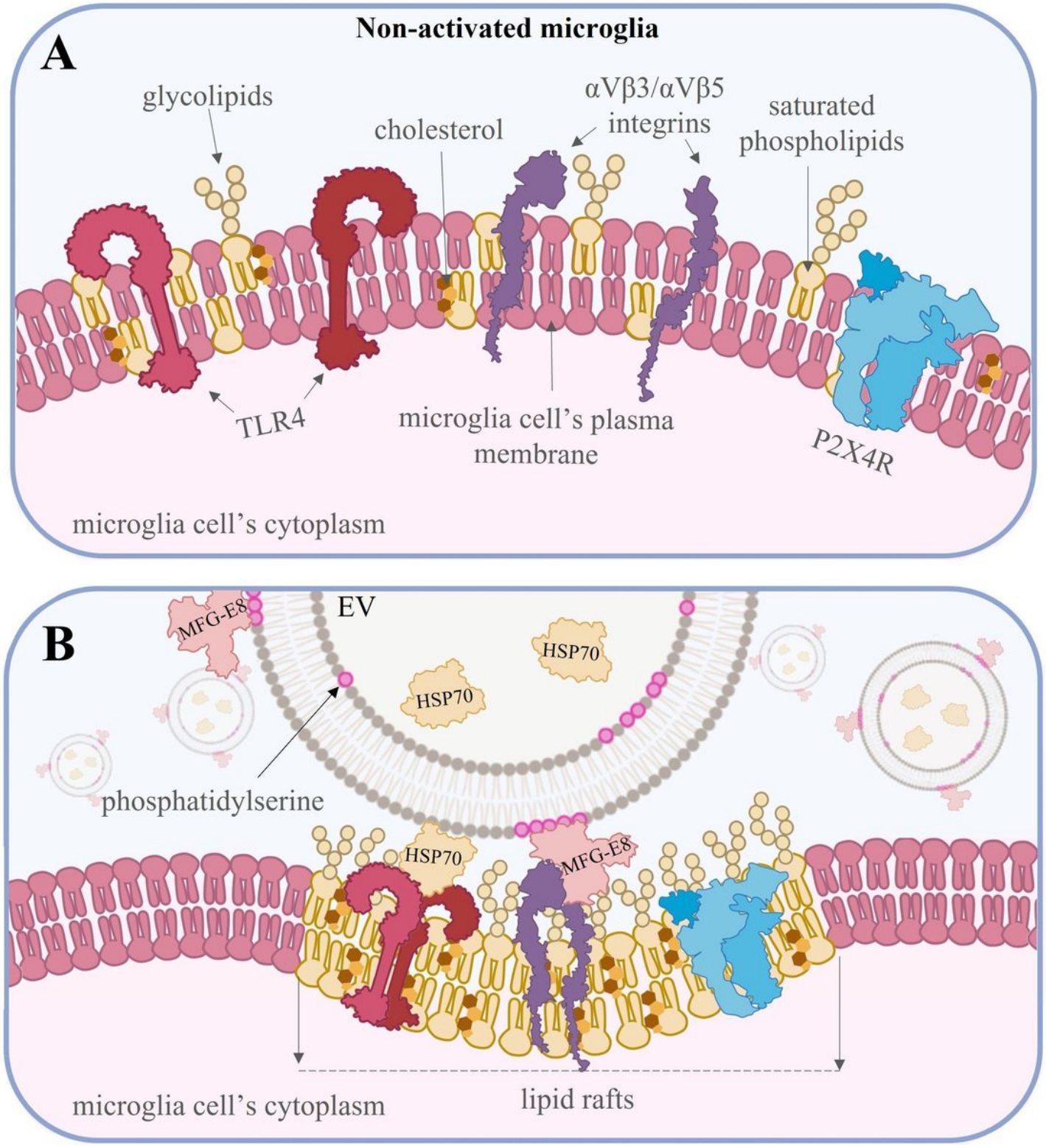

Figure 6

Proposed mechanism for EV action on microglial cells

Supplementary Files

This is a list of supplementary files associated with this preprint. Click to download.

- Supplements.pdf
- Supplementaryfigure1.jpg
- Supplementaryfigure2.jpg